Bull. Chem. Soc. Ethiop. **2023**, 37(2), 449-461.
DOI: https://dx.doi.org/10.4314/bcse.v37i2.14

ISSN 1011-3924
Printed in Ethiopia
Online ISSN 1726-801X

COMPUTATIONAL MOLECULAR DOCKING AND *IN SILICO* ADMET PREDICTION STUDIES OF PYRAZOLE DERIVATIVES AS COVID-19 MAIN PROTEASE (M^{PRO}) AND PAPAIN-LIKE PROTEASE (PL^{PRO}) INHIBITORS

Tamer K. Khatab and Ashraf S. Hassan*

Organometallic and Organometalloid Chemistry Department, National Research Centre, Dokki, 12622, Cairo, Egypt

(Received August 9, 2022; Revised October 1, 2022; Accepted October 22, 2022)

ABSTRACT. The inhibition of severe acute respiratory syndrome coronavirus 2 (SARS-CoV-2) main protease (M^{pro}) and papain-like protease (PL^{pro}) prevents viral multiplications. Molecular docking, absorption, distribution, metabolism, excretion, and toxicity (ADMET) studies of pyrazole-indole molecules **6a, b,** Schiff bases **8a, b,** and pyrazolo[1,5-*a*]pyrimidines **10a, b** were performed and done. Based on the molecular docking study verified that the presented structures (**6a**, **6b**, **8a**, **8b**, **10a**, and **10b**) give promised attached bonds with the active site in the COVID-19 main protease (M^{pro}). The results of *in silico* ADMET prediction study revealed that these compounds may be considered candidates for the discovery or development of new series of COVID-19 drugs.

KEY WORDS: Pyrazole, Fused pyrazole, Schiff bases, COVID-19, Molecular docking, Computational studies

INTRODUCTION

Recently, there is a growing interest in the preparation of pyrazole and fused pyrazole due to their biological applications as antimicrobial, anticancer, antitubercular, and enzyme inhibitors [1-4]. Pyrazolo[1,5-*a*]pyrimidine as an example of fused pyrazole exhibited promising antibacterial activity against *Escherichia coli* and *Salmonella enteric* [5], antitumor activity against colorectal carcinoma (HCT116) and prostate adenocarcinoma (PC-3) [6], and also, the pyrazolo[1,5-*a*]pyrimidine moiety is found in some marketed drugs such as Dinaciclib (SCH-727965), a cyclin-dependent kinases (CDKs) inhibitor that it is being evaluated in clinical trials for various cancer indications [7].

Besides, Schiff bases tethered pyrazole moiety (pyrazole-azomethine) are known to have a vast spectrum of biological activities such as antimicrobial, antitubercular, anthelmintic, antioxidant, analgesic, immunomodulatory, anti-inflammatory, cytotoxic, antiviral, DNA binding, and DHFR/DNA gyrase inhibitors [8-10]. Figure 1 shows the structure of 7-(4-methoxyphenyl)-2-phenylpyrazolo[1,5-*a*]pyrimidine-3,6-dicarbonitrile **(1)** which exhibited antiproliferative activity [11], pyrazole-azomethine-pyrazole **(2)**, 5-((5-chloro-1-(4-fluorophenyl)-3-methyl-1*H*-pyrazol-4-yl)methyleneamino)-1-(4-(trifluoromethyl)phenyl)-1*H*-pyrazole-4-carbonitrile, showed the most potent anti-tobacco mosaic virus (TMV) [12], and finally, isatin **(3)** which exhibited anti-inflammatory activity [13].

Among many disease outbreaks caused by RNA viruses, coronavirus disease 2019 (COVID-19) caused by severe acute respiratory syndrome coronavirus 2 (SARS-CoV-2) is the deadliest of all. Since its initiation in December 2019, COVID-19 has afflicted humans worldwide. Viral enzymes such as the main protease (M^{pro}) and papain-like protease (PL^{pro}) are significantly responsible for the replication of SARS-CoV-2. As inhibition of M^{pro} and PL^{pro} prevents viral multiplication, they have been recognized as the most promising targets for anti-SARS-CoV-2 drugs [14].

*Corresponding author. E-mail: ashraf_salmoon@yahoo.com

Nowadays, molecular modeling study is considered an important study because it provides a more accurate picture of biologically active molecules at the atomic level and plays a major role in the drug designing process [15]. Molecular docking simulation is considered the simplified form of molecular dynamic (MD) simulation that safe time and money spent and common component of drug discovery because traditional experimental methods for drug discovery take a long time [16]. Docking study can also be defined as a computational procedure that studies how ligand and protein fit both energetically and geometrically to give us a complete figure to predict the binding-conformation of small drug-like molecules to target proteins [17]. Molecular docking simulation was used to predict the possible binding mode as well as the active conformation of these derivatives inside the target enzyme. Additionally, the preferring structure selected from one to another in the docking study related to the highest binding affinity between the ligand and the protein [18].

From the above facts and in continuation of our targets [19-26], the presented work aims to study the molecular docking of pyrazole-indole molecules **6a,b,** Schiff bases **8a,b,** and pyrazolo[1,5-*a*]pyrimidines **10a,b** as COVID-19 main protease (M^{pro}) and papain-like protease (PL^{pro}) inhibitors. Also, the work extended to study the *in silico* absorption, distribution, metabolism, excretion, and toxicity (ADMET).

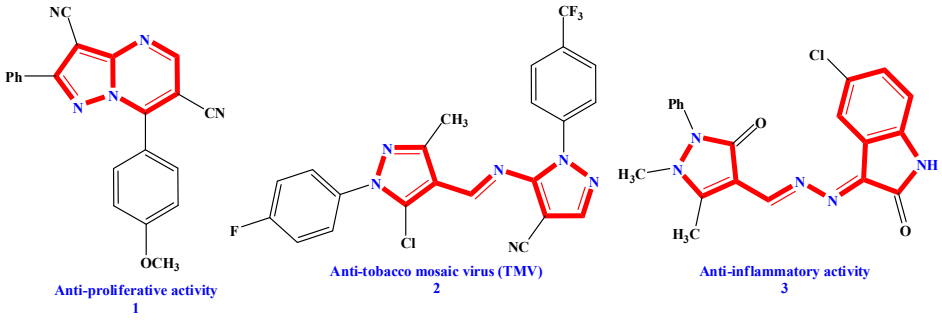

Figure 1. Bioactivity of fused pyrazole and pyrazole-azomethine compounds **1-3**.

EXPERIMENTAL

Synthesis of 5-amino-3-(arylamino)-1H-pyrazole-4-carboxamides **4a-e** [27]

Compounds of this series were prepared according to the literature procedure.

*5-Amino-N-phenyl-3-(phenylamino)-1H-pyrazole-4-carboxamide (**4a**)*. White, m.p. 247 °C. ^{1}H NMR (DMSO-d_6, δ ppm) 6.01 (s, 2H, NH_2), 6.76-7.48 (m, 10H, $2C_6H_5$), 8.52 (s, 1H, NH), 8.73 (s, 1H, NH), 11.32 (s, 1H, NH) [27].

*5-Amino-3-(phenylamino)-N-(4-methylphenyl)-1H-pyrazole-4-carboxamide (**4b**)*. White, m.p. 178 °C. ^{1}H NMR (DMSO-d_6, δ ppm) 2.23 (s, 3H, CH_3), 5.98 (s, 2H, NH_2), 7.05-7.37 (m, 9H, C_6H_4 and C_6H_5), 8.54 (s, 1H, NH), 8.64 (s, 1H, NH), 11.29 (s, 1H, NH) [27].

*5-Amino-3-[(4-methoxyphenyl)amino]-N-phenyl-1H-pyrazole-4-carboxamide (**4c**)*. White crystals, m.p. 175-177 °C. ^{1}H NMR (DMSO-d_6, δ ppm) 3.63 (s, 3H, OCH_3), 5.98 (s, 2H, NH_2, D_2O exchangeable), 6.76 (d, 2H, aromatic, J_{HH} = 7.7 Hz), 6.98 (t, 1H, aromatic, J_{HH} = 7.7 Hz), 7.18 (t, 2H, aromatic, J_{HH} = 8.4 Hz), 7.25 (d, 2H, aromatic, J_{HH} = 7.7 Hz), 7.45 (d, 2H, aromatic, J_{HH} = 7.7 Hz), 8.30 (s, 1H, NH, D_2O exchangeable), 8.74 (s, 1H, NH, D_2O exchangeable), 11.22

(s, 1H, NH, D_2O exchangeable). ^{13}C NMR (DMSO-d_6, δ ppm) 55.6 (-OCH_3), 88.3 (C_4, pyrazole), 114.7, 117.5, 120.3, 123.3, 129.1, 137.6, 139.4 (11C, aromatic), 149.1 (C_5, pyrazole), 150.9 (C_3, pyrazole), 153.1 (C, aromatic), 163.6 (C=O) [27].

5-Amino-3-[(4-methoxyphenyl)amino]-N-(4-methylphenyl)-1H-pyrazole-4-carboxamide ***(4d)***. White crystals, m.p. 198-200 °C. ^1H-NMR (DMSO-d_6, δ ppm) 2.21 (s, 3H, CH_3), 3.64 (s, 3H, OCH_3), 5.95 (s, 2H, NH_2, D_2O exchangeable), 6.76 (d, 2H, aromatic, J_{HH} = 8.4 Hz), 7.04 (d, 2H, aromatic, J_{HH} = 8.4 Hz), 7.16 (d, 2H, aromatic, J_{HH} = 8.4 Hz), 7.33 (d, 2H, aromatic, J_{HH} = 8.4 Hz), 8.30 (s, 1H, NH, D_2O exchangeable), 8.66 (s, 1H, NH, D_2O exchangeable), 11.21 (s, 1H, NH, D_2O exchangeable) [27].

5-Amino-N-(4-chlorophenyl)-3-[(4-methoxyphenyl)amino]-1H-pyrazole-4-carboxamide ***(4e)***. White crystals, m.p. 190-192 °C. ^1H NMR (DMSO-d_6, δ ppm) 3.64 (s, 3H, OCH_3), 6.00 (s, 2H, NH_2, D_2O exchangeable), 6.77-7.51 (m, 8H, aromatic), 8.30 (s, 1H, NH, D_2O exchangeable), 8.82 (s, 1H, NH, D_2O exchangeable), 11.20 (s, 1H, NH, D_2O exchangeable). ^{13}C NMR (DMSO-d_6, δ ppm) 55.7 (-OCH_3), 87.9 (C_4, pyrazole), 114.7, 117.7, 121.9, 126.8, 128.9, 137.4, 138.4 (11C, aromatic), 149.1 (C_5, pyrazole), 151.1 (C_3, pyrazole), 153.2 (C, aromatic), 163.6 (C=O) [27].

Synthesis of pyrazole-indole molecules **6a,b** [28]

The target compounds, pyrazole-indole molecules **6a,b** were prepared according to the method described in our work.

5-((1H-Indol-3-yl)methyleneamino)-N-phenyl-3-(phenylamino)-1H-pyrazole-4-carboxamide ***(6a)***. Yellow crystals, m.p. 266-268 °C. ^1H NMR (DMSO-d_6, δ ppm) 6.87 (t, 1H, J = 7.3 and 7.3 Hz, ArH), 7.07 (t, 1H, J = 7.4 and 7.4 Hz, ArH), 7.24-7.37 (m, 6H, ArH), 7.57-7.65 (m, 5H, ArH), 8.33 (s, 1H, indole), 8.35 (d, 1H, J = 7.9 Hz, ArH), 9.00 (s, 1H, -N=CH-), 9.06 (s, 1H, NH), 10.03 (s, 1H, NH), 12.30 (s, 2H, 2NH). ^{13}C NMR (DMSO-d_6, δ ppm) 92.05 (C, C_4-pyrazole), 112.99, 114.34, 116.44, 119.42, 119.82, 121.23, 122.07, 123.33, 123.90, 124.35, 128.63, 128.98, 129.02, 137.73, 138.57, 141.36 (20C, Ar), 149.74 (C, C_5-pyrazole), 152.03 (C, C_3-pyrazole), 158.89 (C, -N=C-), 163.29 (C, C=O) [28].

5-((1H-Indol-3-yl)methyleneamino)-3-(phenylamino)-N-(4-methylphenyl)-1H-pyrazole-4-carboxamide ***(6b)***. Yellow crystals, m.p. 276-278 °C. ^1H NMR (DMSO-d_6, δ ppm) 2.27 (s, 3H, CH_3), 6.87 (t, 1H, J = 7.3 and 7.3 Hz, ArH), 7.14 (d, 2H, J = 8.3 Hz, ArH), 7.24-7.31 (m, 3H, ArH), 7.35 (t, 1H, J = 7.1 and 7.0 Hz, ArH), 7.53 (d, 2H, J = 8.4 Hz, ArH), 7.57 (d, 2H, J = 8.2 Hz, ArH), 7.60 (d, 1H, J = 8.1 Hz, ArH), 8.33 (s, 1H, indole), 8.34 (d, 1H, J = 7.6 Hz, ArH), 9.00 (s, 1H, -N=CH-), 9.05 (s, 1H, NH), 9.96 (s, 1H, NH), 12.29 (s, 2H, 2NH). ^{13}C NMR (DMSO-d_6, δ ppm) 20.38 (C, CH_3), 92.02 (C, C_4-pyrazole), 112.94, 114.28, 116.34, 119.35, 121.18, 122.02, 123.84, 124.27, 128.98, 129.31, 132.27, 135.99, 137.66, 139.39, 141.34, 149.44 (20C, Ar), 153.15 (C, C_5-pyrazole), 155.63 (C, C_3-pyrazole), 158.66 (C, -N=C-), 163.09 (C, C=O) [28].

Synthesis of Schiff bases **8a,b** [29]

Compounds of this series were prepared according to the literature procedure.

5-(Benzylideneamino)-3-(4-methoxyphenylamino)-N-(4-methylphenyl)-1H-pyrazole-4-carboxamide ***(8a)***. Orange crystals, mp 225 ºC. IR (KBr) ν_{max}/cm^{-1} 3431, 3294 (NH), 1648 (C=O). ^1H NMR (DMSO-d_6, δ ppm) 2.27 (3H, s, CH_3), 3.72 (3H, s, OCH_3), 6.90 (2H, d, J = 8.9 Hz, ArH), 7.17 (2H, d, J = 8.3 Hz, ArH), 7.40 (2H, ArH), 7.55 (2H, d, J = 8.4 Hz, ArH), 7.63-7.65 (3H, m, ArH), 8.06 (2H, d, J = 7.8 Hz, ArH), 8.71 (1H, s, -N=CH-), 9.07 (1H, s, NH), 9.86 (1H,

s, NH), 12.70 (1H, s, NH). ^{13}C NMR (DMSO-d_6, δ ppm) 20.86 (CH_3), 55.78 (OCH_3), 93.57 (C_4, pyrazole), 115.89, 120.42, 120.51, 129.98, 130.12, 130.84, 132.86, 133.07, 134.92, 136.18, 137.64, 153.43 (18C, Ar), 153.84 (C_5, pyrazole), 156.63 (C_3, pyrazole), 160.18 (-N=CH-), 163.02 (C=O) [29].

*5-(Benzylideneamino)-N-(4-chlorophenyl)-3-(4-methoxyphenylamino)-1H-pyrazole-4-carboxamide (**23**)*. Yellow crystals, m.p. 210 ºC. IR (KBr) ν_{max}/cm^{-1} 3425, 3298 (NH), 1642 (C=O). ^{1}H NMR (DMSO-d_6, δ ppm) 3.73 (3H, s, OCH_3), 6.91 (2H, d, J = 8.3 Hz, ArH), 7.26-7.43 (5H, m, ArH), 7.64 (2H, d, J = 7.3 Hz, ArH), 7.70 (2H, d, J = 8.8 Hz, ArH), 8.07 (2H, d, J = 6.5 Hz, ArH), 8.66 (1H, s, -N=CH-), 9.06 (1H, s, NH), 9.96 (1H, s, NH), 12.76 (1H, s, NH). ^{13}C NMR (DMSO-d_6, δ ppm) 55.72 (OCH_3), 92.36 (C_4, pyrazole), 115.25, 120.34, 120.79, 129.80, 130.31, 130.89, 131.21, 132.62, 135.36, 136.79, 152.62 (18C, Ar), 153.23 (C_5, pyrazole), 155.41 (C_3, pyrazole), 160.79 (-N=CH-), 163.19 (C=O) [29].

Synthesis of pyrazolo[1,5-a]pyrimidines **10a,b** [30]

The target compounds were prepared according to the method described in our work.

2-(4-Methoxyphenylamino)-N,7-diphenylpyrazolo[1,5-a]pyrimidine-3-carboxamide (***10a***). Yellow crystals, m.p. 218-220 °C. IR (KBr) ν_{max}/cm^{-1} 3346 (NH), 1658 (C=O). ^{1}H NMR ($CDCl_3$, δ ppm) 3.80 (s, 3H, OCH_3), 6.88 (d, 2H, J = 9.0 Hz, ArH), 6.96 (d, 1H, J = 4.8 Hz, pyrimidine), 7.12 (t, 1H, ArH), 7.36-7.42 (m, 5H, ArH), 7.62 (d, 2H, J = 9.0 Hz, ArH), 7.74 (d, 2H, J = 8.4 Hz, ArH), 8.11 (d, 2H, J = 8.3 Hz, ArH), 8.49 (d, 1H, J = 4.8 Hz, pyrimidine), 9.40 (s, 1H, NH), 10.05 (s, 1H, NH). ^{13}C NMR ($CDCl_3$, δ ppm) 55.7 (C, OCH_3), 87.8 (C, C_3-pyrazolopyrimidine), 107.0 (C, C_6-pyrazolopyrimidine), 114.4, 119.2, 120.2, 123.7, 127.7, 129.1, 129.5, 129.6 (14C, Ar), 134.1 (C, C_{3a}-pyrazolopyrimidine), 138.8, 142.4, 146.7 (3C, Ar), 147.9 (C, C_7-pyrazolopyrimidine), 149.6 (C, Ar), 154.5 (C, C_2-pyrazolopyrimidine), 157.8 (C, C_5-pyrazolopyrimidine), 163.3 (C=O) [30].

*N-(4-Chlorophenyl)-2-(4-methoxyphenylamino)-7-phenylpyrazolo[1,5-a]pyrimidine-3-carboxamide (**10b**)*. Yellow crystals, m.p. 252-254 °C. IR (KBr) ν_{max}/cm^{-1} 3336 (NH), 1650 (C=O). ^{1}H NMR (DMSO-d_6, δ ppm) 3.72 (s, 3H, OCH_3), 6.90 (d, 2H, J = 9.0 Hz, ArH), 7.40 (d, 1H, J = 4.8 Hz, pyrimidine), 7.44 (d, 2H, J = 8.8 Hz, ArH), 7.61 (d, 2H, J = 9.0 Hz, ArH), 7.68-7.70 (m, 3H, ArH), 7.78 (d, 2H, J = 8.9 Hz, ArH), 8.23 (d, 2H, J = 7.2 Hz, ArH), 8.75 (d, 1H, J = 4.8 Hz, pyrimidine), 9.20 (s, 1H, NH), 10.11 (s, 1H, NH). ^{13}C NMR (DMSO-d_6, δ ppm) 55.7 (C, OCH_3), 87.9 (C, C_3-pyrazolopyrimidine), 107.0 (C, C_6-pyrazolopyrimidine), 114.5, 119.1, 120.2, 124.0, 128.4, 129.1, 130.9, 131.8 (13C, Ar), 134.0 (C, C_{3a}-pyrazolopyrimidine), 134.6, 135.9, 138.0, 138.7 (4C, Ar), 145.6 (C, C_7-pyrazolopyrimidine), 149.7 (C, Ar), 154.8 (C, C_2-pyrazolopyrimidine), 158.0 (C, C_5-pyrazolopyrimidine), 163.8 (C=O) [30].

MOE "molecular docking"

On the bases of the standard docking protocol using MOE2015.10 software the X-ray crystallographic structure of the COVID-19 main protease (M^{pro}) inhibitor (PDB ID: 7BUY). The Molecular Operating, E.; Chemical Computing Group I.; Montreal QC. In.; 2016.

Docking protocol molecular docking protocols are widely used for predicting the binding affinities for a number of ligands. In the current work, our aim was to examine the possibility of an existing relationship between the experimental bioactivities of the inhibitors under study and the docking scores. In order to get accurate results, all the docking experiments were performed with the default parameters. The time to dock one ligand was approximately 1–2 min. Docking with AutoDock/Vina, GOLD, and FRED was performed on a Linux workstation (openSUSE11.4)

with an Intel Pentium D processor (3.0 GHz) and 1 GB of RAM whereas FlexX was run on windows 7 equipped with an Intel® Atom™ processor (1.67 GHz) and 1GB of RAM.

ADMET prediction properties

Absorption, distribution, metabolism, excretion, and toxicity (ADMET) prediction properties of pyrazole-indole molecules **6a,b**, Schiff bases **8a,b**, and pyrazolo[1,5-*a*]pyrimidines **10a,b** were predicted using pkCSM web [31].

RESULTS AND DISCUSSION

Chemistry

The starting materials, 5-aminopyrazoles **4a-e**, were synthesized according to the reported method [27]. The two pyrazole-indole molecules **6a,b** were prepared by the reaction of **4a,b** with 1*H*-indole-3-carbaldehyde (**5**) in refluxing ethanol in the presence of a catalytic amount of AcOH acid [28]. Also, the two Schiff bases **8a,b** were synthesized by the condensation of **4d,e** with benzaldehyde (**7**) [29]. Pyrazolo[1,5-*a*]pyrimidines **10a,b** were prepared *via* the condensation of **4c,e** with 3-(dimethylamino)-1-phenyl-prop-2-en-1-one (**9**) in refluxing AcOH [30] (Scheme 1).

Molecular docking study

Molecular docking validations were done to predict the binding between active sites in the COVID-19 main protease (M^{pro}) as a targeting enzyme docked by pyrazoles. The result was obtained by comparison with hydroxychloroquine as a reference molecule. Hydroxychloroquine during the last few months was considered a promised candidate drug for Covid-19 [32]. The inhibition of M^{pro} presents a unique challenge in which the active site pocket is characteristically and in continuation of our work [33] to discover new drug enzyme interaction we presented this study.

The root-mean-square deviation (RMSD) and *E-score* (energy score in kcal/mol) are considered significant factors that explained the binding process between the ligand and enzyme. The molecular docking validation clarifies the interaction (*E-score*) between pyrazole-indole molecules **6a,b**, Schiff bases **8a,b**, and pyrazolo[1,5-*a*]pyrimidines **10a,b** with a M^{pro} enzyme (Table 1). The calculated data explained that the protease active site protein residues are Asn 142, Thr 45, Thr 26, Glu 166, His 41, Thr 25, Gln 192, Thr 190, Arg 188, Ala 191, Met 165, Leu 167, Leu 141, Asp 187, Thr 42, Pro 168, His 164, Gly 143, Ser 144, Cys 145, Gln 189, Met 49, Leu 27, Ser 46, and Cys 44. Figures 2a and 2b show the 2D and 3D interaction diagrams with M^{pro}.

Table 1. Energy score and the root-mean-square deviation (RMSD).

	6a	**6b**	**10a**	**10b**	**8a**	**8b**
E-score (kcal/mol)	-7.89	-7.55	-7.33	-7.49	-7.74	-7.37
RMSD	0.68	1.03	1.06	1.05	1.50	0.95

The drug-ligand electrostatic force distance measurements

The measured distance also reflects the good drug ligand interaction. For example, we presented the drug-ligand electrostatic force-distance measurements for compounds (**6a, 6b, 8a, 8b, 10a,** and **10b**) the hydrogen bond distance between Thr 26 and bromo group equal to 3.31; the π-π stacking also presented between Gln 189 and Met 49 with the two aromatic rings. This compound presented **6a** intramolecular forces that presented the high drug ligand interaction.

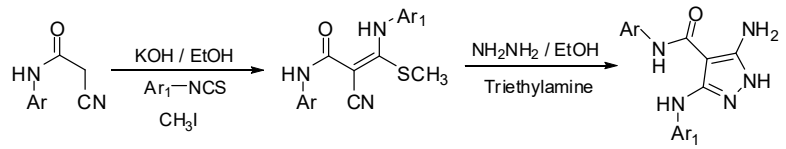

4a; Ar= C_6H_5, Ar_1= C_6H_5
4b; Ar= 4-CH_3-C_6H_4, Ar_1= C_6H_5
4c; Ar= C_6H_5, Ar_1= 4-OCH_3-C_6H_4
4d; Ar= 4-CH_3-C_6H_4, Ar_1= 4-OCH_3-C_6H_4
4e; Ar= 4-Cl-C_6H_4, Ar_1= 4-OCH_3-C_6H_4

4a-e

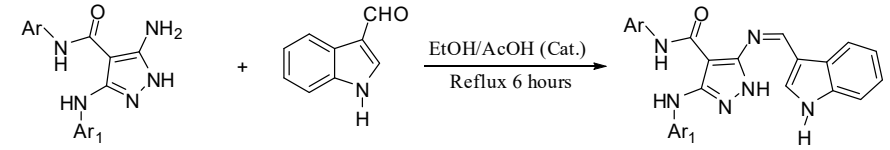

4a, b

5

6a, b

4a; Ar= C_6H_5, Ar_1= C_6H_5
4b; Ar= 4-CH_3-C_6H_4, Ar_1= C_6H_5

6a; Ar= C_6H_5, Ar_1= C_6H_5
6b; Ar= 4-CH_3-C_6H_4, Ar_1= C_6H_5

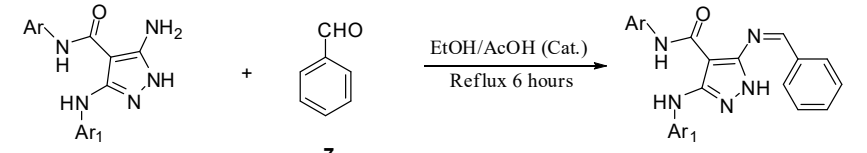

4d, e

7

8a, b

4d; Ar= 4-CH_3-C_6H_4, Ar_1= 4-OCH_3-C_6H_4
4e; Ar= 4-Cl-C_6H_4, Ar_1= 4-OCH_3-C_6H_4

8a; Ar= 4-CH_3-C_6H_4, Ar_1= 4-OCH_3-C_6H_4
8b; Ar= 4-Cl-C_6H_4, Ar_1= 4-OCH_3-C_6H_4

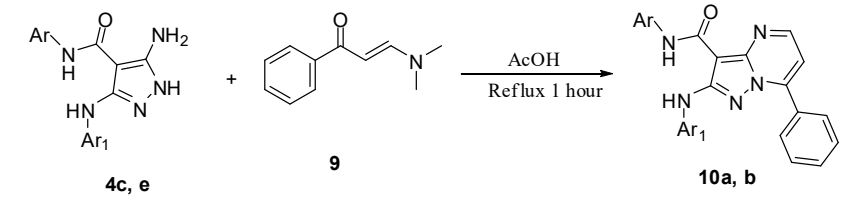

4c, e

9

10a, b

4c; Ar= C_6H_5, Ar_1= 4-OCH_3-C_6H_4
4e; Ar= 4-Cl-C_6H_4, Ar_1= 4-OCH_3-C_6H_4

10a; Ar= C_6H_5, Ar_1= 4-OCH_3-C_6H_4
10b; Ar= 4-Cl-C_6H_4, Ar_1= 4-OCH_3-C_6H_4

Scheme 1. Synthesis of 5-aminopyrazoles **4a–e** and pyrazole derivatives **6a,b, 8a,b**, and **10a,b**.

The molecular docking validation clarifies the interaction (*E-score*) between pyrazole-indole molecules **6a,b**, Schiff bases **8a,b**, and pyrazolo[1,5-*a*]pyrimidines **10a,b** with a PL^{pro} enzyme (Table 2). The calculated data explained that the protease active site protein residues are Tyr 273, Pro 247, Lys 157, Met 208, Leu 162, Pro 248, Tyr 268, Tyr 264, Asp 164, Gin 269, Glu 161, Gly 163, Tle 301, Glu 167, and Erg 166. Figure 3 showed the 2D interaction diagrams with papain-like protease (PL^{pro}).

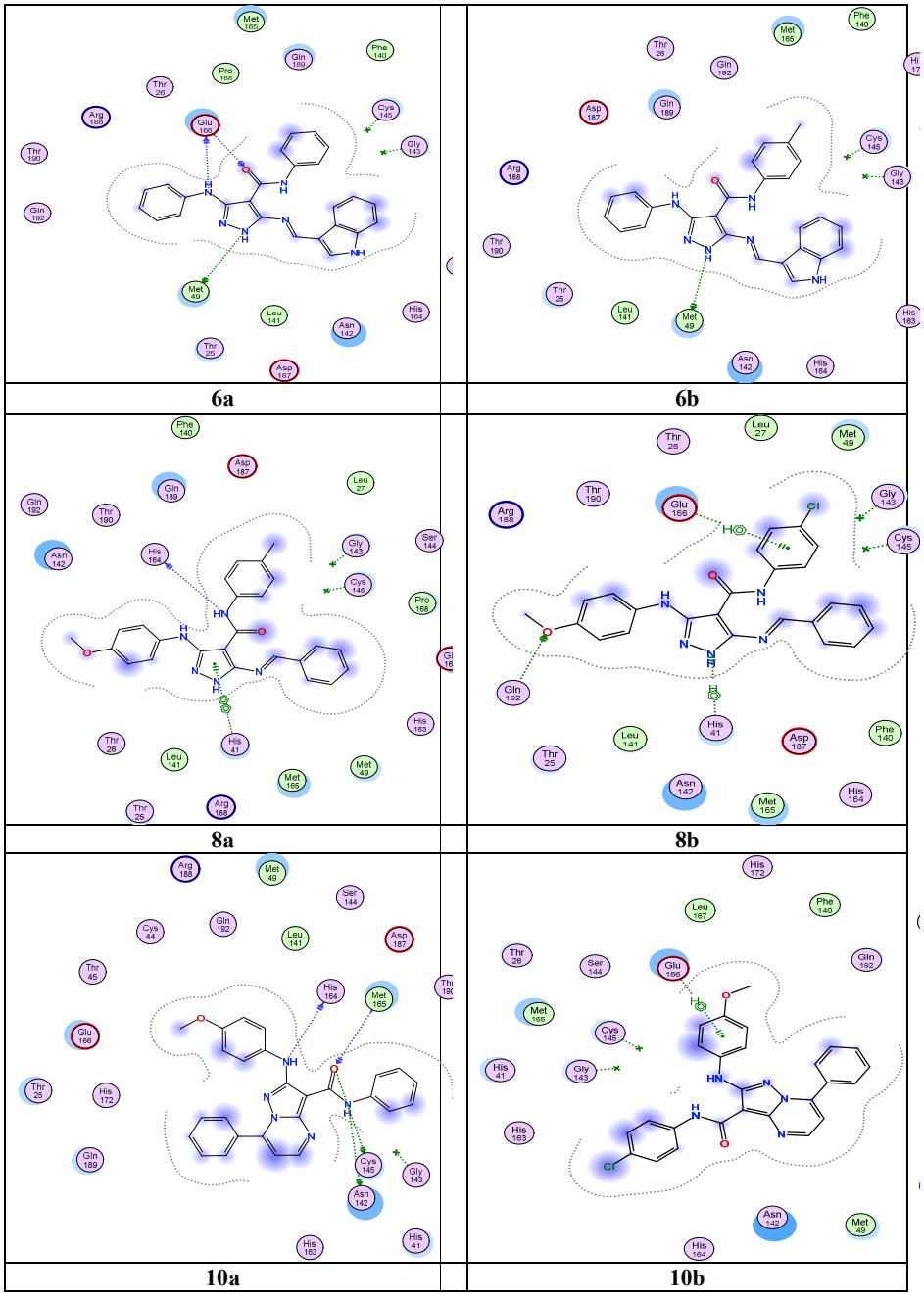

Figure 2a. 2D of the drug ligand interaction between (**6a**, **6b**, **8a**, **8b**, **10a**, **and 10b**) and M^{pro} enzyme active side.

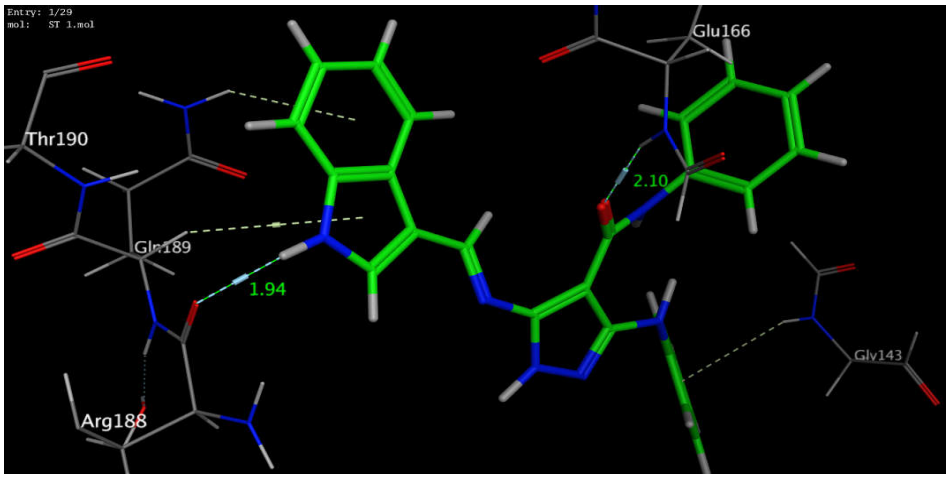

Figure 2b. The distance measurements in 3D interaction diagrams of **6a** with M^{pro} enzyme binding active side.

Table 2. Energy score and the root-mean-square deviation (RMSD).

	6a	**6b**	**10a**	**10b**	**8a**	**8b**
E-score (kcal/mol)	-6.72	-6.13	-6.53	-6.65	-6.36	-6.33
RMSD	1.35	1.28	1.31	1.98	1.48	1.18

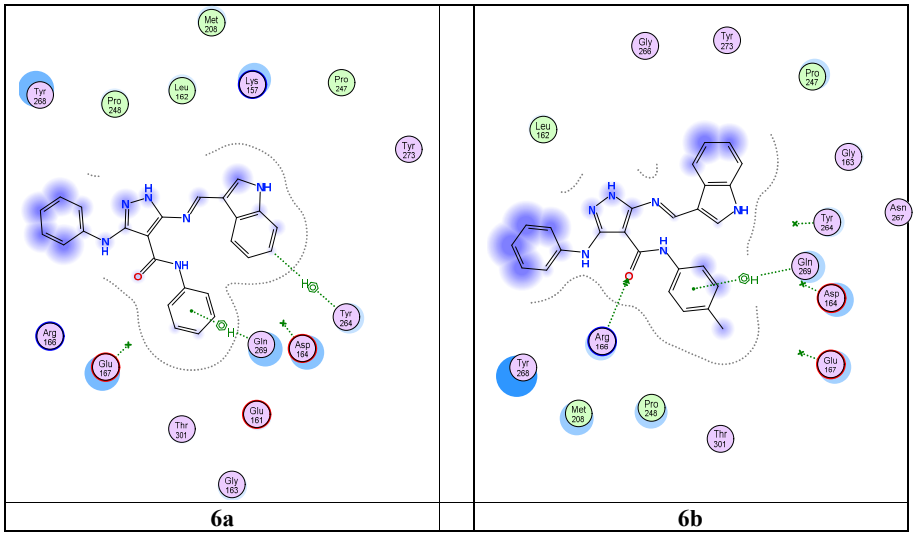

6a **6b**

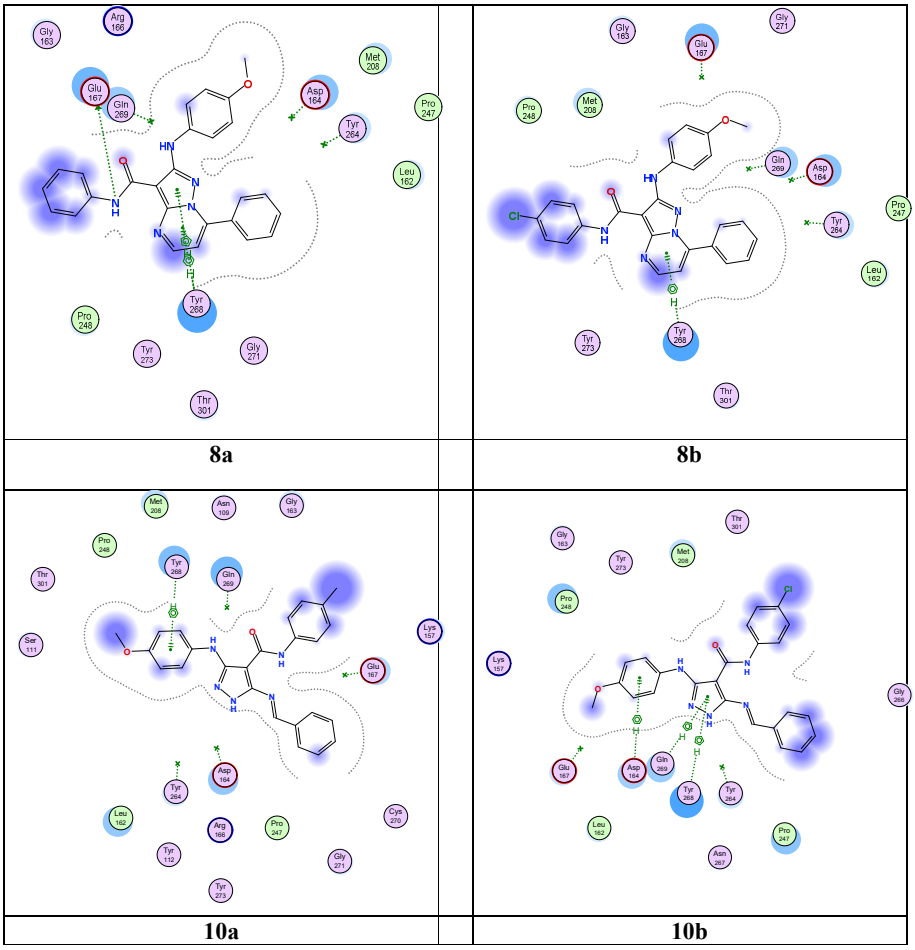

Figure 3. 2D of the drug ligand interaction between (**6a**, **6b**, **8a**, **8b**, **10a**, and **10b**) and PL^{pro} enzyme active side.

In silico ADMET prediction

The absorption, distribution, metabolism, excretion, and toxicity (ADMET) prediction properties of pyrazole-indole molecules **6a,b**, Schiff bases **8a,b**, and pyrazolo[1,5-*a*]pyrimidines **10a,b** were predicted using pkCSM web (http://biosig.unimelb.edu.au/pkcsm/prediction) [31]. The results properties are shown in Table 3.

Absorption properties, P-gps substrate or enzymes (P-glycoprotein substrate, P-glycoprotein I inhibitor, and P-glycoprotein II inhibitor) are the keys to estimating active efflux through biological membranes and are known as the most important member of ATP-binding cassette transporters or ABC-transporters used to protect the central nervous system (CNS) from xenobiotics. From the result, we can conclude that all the molecules **6a**, **6b**, **8a**, **8b**, **10a**, and **10b** are inhibitors for P-glycoprotein substrate, P-glycoprotein I enzyme, and P-glycoprotein II enzyme.

The distribution properties are including the blood-brain barrier (BBB) Permeability, central nervous system (CNS) Permeability, and volume of distribution (VDss) [34]. The BBB permeability values, the four compounds, pyrazole-indole molecules **6a,b**, and Schiff bases **8a,b**, have lower values of log BB (log BB < -1, ranging between -1.47 to -1.624) referring to these compounds are poorly distributed to the brain and have not the ability to pass the blood-brain barrier (BBB). But, pyrazolo[1,5-*a*]pyrimidines **10a** and **10b** have values of log BB -0.073 and -0.234, respectively, which refer to these compounds are moderately distributed. The six compounds **6a**, **6b**, **8a**, **8b**, **10a**, and **10b** have CNS permeability of more than -2; therefore, these compounds have the ability to penetrate the central nervous system (CNS). The volume of distribution (VDss) predicted that all the molecules **6a**, **6b**, **8a**, **8b**, **10a**, and **10b** have lower values of VDss (log VDss < -0.15, ranging between -0.832 to -0.319) refer to the compounds are contained in plasma rather than in tissues.

Inhibition of the five major CYP isoforms (CYP1A2, CYP2C19, CYP2C9, CYP2D6, and CYP3A4) is certainly one major cause of pharmacokinetics-related drug-drug interactions leading to toxic or other unwanted adverse effects due to the lower clearance and accumulation of the drug or its metabolites [35]. All the molecules **6a**, **6b**, **8a**, **8b**, **10a**, and **10b** are inhibitors of the CYP1A2, CYP2C19, and CYP2C9 enzymes. But, are non-inhibitors of the CYP2D6 enzyme. The four molecules **8a**, **8b**, **10a**, and **10b** are inhibitors of the CYP3A4 enzyme, but, the two compounds **6a** and **6b** are non-inhibitors.

To determine the excretion routes, renal organic cation transporter 2 (OCT2) substrate was predicted. Results showed that all the compounds **6a**, **6b**, **8a**, **8b**, **10a**, and **10b** are non-inhibitors of renal organic cation transporter 2 (OCT2).

Hepatotoxicity (from hepatic toxicity) implies chemical-driven liver damage. Drug-induced liver injury is a cause of acute and chronic liver disease caused specifically by medications. The five compounds **6a**, **8a**, **8b**, **10a**, and **10b** are inhibitors for the compounds that caused hepatic toxicity except for **6b**. hERG I and II inhibitors: inhibition of the potassium channels encoded by hERG (human ether-a-go-go-related gene) is the principal cause for the development of acquiring long QT syndrome-leading to fatal ventricular arrhythmia. All the molecules are non-inhibitors of the hERG I enzyme but are inhibitors of the hERG II enzyme.

Table 3. The absorption, distribution, metabolism, excretion, and toxicity (ADMET) prediction properties of pyrazole-indole molecules **6a,b**, Schiff bases **8a,b**, and pyrazolo[1,5-*a*]pyrimidines **10a,b**.

ADMET properties	**6a** [31]	**6b**	**8a**	**8b**	**10a**	**10b**
Absorption						
P-glycoprotein substrate Yes; substrate, No; non-substrate	Yes	Yes	Yes	Yes	Yes	Yes
P-glycoprotein I inhibitor Yes; inhibitor, No; non-inhibitor	Yes	Yes	Yes	Yes	Yes	Yes
P-glycoprotein II inhibitor Yes; inhibitor, No; non-inhibitor	Yes	Yes	Yes	Yes	Yes	Yes
Distribution						
BBB Permeability (log BB) Log BB>0.3 (high), log BB<-1 (poor)	-1.581	-1.602	-1.47	-1.624	-0.073	-0.234
CNS Permeability (log PS) log PS>-2 (penetrate), log PS<-3 (unable)	-1.782	-1.713	-1.901	-1.861	-1.811	-1.701
VDss (human) log VDss>0.45 (high), log VDss<-0.15 (low)	-0.832	-0.801	-0.667	-0.684	-0.381	-0.319
Metabolism						
CYP1A2 enzyme Yes; inhibitor, No; non-inhibitor	Yes	Yes	Yes	Yes	Yes	Yes

CYP2C19 enzyme Yes; inhibitor, No; non-inhibitor	Yes	Yes	Yes	Yes	Yes	Yes
CYP2C9 enzyme Yes; inhibitor, No; non-inhibitor	Yes	Yes	Yes	Yes	Yes	Yes
CYP2D6 enzyme Yes; inhibitor, No; non-inhibitor	No	No	No	No	No	No
CYP3A4 enzyme Yes; inhibitor, No; non-inhibitor	No	No	Yes	Yes	Yes	Yes
Excretion						
Renal OCT2 substrate Yes; substrate, No; non- substrate	No	No	No	No	No	No
Toxicity						
Hepatotoxicity Yes; inhibitor, No; non-inhibitor	Yes	No	Yes	Yes	Yes	Yes
hERG I inhibitor Yes; inhibitor, No; non-inhibitor	No	No	No	No	No	No
hERG II inhibitor Yes; inhibitor, No; non-inhibitor	Yes	Yes	Yes	Yes	Yes	Yes

CONCLUSION

The aim of this manuscript was to study the molecular docking of pyrazole-indole molecules **6a,b**, Schiff bases **8a,b**, and pyrazolo[1,5-*a*]pyrimidines **10a,b** as COVID-19 main protease (M^{pro}) and papain-like protease (PL^{pro}) inhibitors. Also, study *in silico* absorption, distribution, metabolism, excretion, and toxicity (ADMET) prediction properties. The molecular docking study verified that the presented structures (**6a**, **6b**, **8a**, **8b**, **10a**, and **10b**) give promised attached bonds with the active site in the COVID-19 main protease (M^{pro}). *In silico* ADMET prediction study revealed that all the molecules **6a**, **6b**, **8a**, **8b**, **10a**, and **10b** are inhibitors for P-glycoprotein substrate, P-glycoprotein I enzyme, and P-glycoprotein II enzyme, have CNS permeability of more than -2, have lower values of VDss (log VDss < -0.15, ranged between -0.832 to -0.319), and are inhibitors of the CYP1A2, CYP2C19, CYP2C9, and hERG II enzymes but are non-inhibitors of the CYP2D6, renal organic cation transporter 2 (OCT2), and hERG I enzymes. (ii) The four compounds, **6a**, **6b**, **8a**, and **8b**, have lower values of log BB (log BB < -1, ranging between -1.47 to -1.624). But, pyrazolo[1,5-*a*]pyrimidines **10a** and **10b** have values of log BB -0.073 and -0.234, respectively. (iii) The four molecules **8a**, **8b**, **10a**, and **10b** are inhibitors of the CYP3A4 enzyme, but, the two compounds **6a** and **6b** are non-inhibitors. (iv) The five compounds **6a**, **8a**, **8b**, **10a**, and **10b** are inhibitors for the compounds that caused hepatic toxicity except for **6b**. In the future, this study could be valuable in the discovery of new series of COVID-19 drugs by modification the structure of the molecules.

ACKNOWLEDGMENT

The authors wish to present thanks to the National Research Centre, Dokki, Cairo, Egypt for the facilities provided.

REFERENCES

1. Hassan, A.S.; Morsy, N.M.; Awad, H.M.; Ragab, A. Synthesis, molecular docking, and in silico ADME prediction of some fused pyrazolo[1,5-*a*]pyrimidine and pyrazole derivatives as potential antimicrobial agents. *J. Iran. Chem. Soc*. **2022**, 19, 521-545.
2. Mukhtar, S.S.; Hassan, A.S.; Morsy, N.M.; Hafez, T.S.; Saleh, F.M.; Hassaneen, H.M. Design, synthesis, molecular prediction and biological evaluation of pyrazole-azomethine conjugates as antimicrobial agents. *Synth. Commun.* **2021**, 51, 1564-1580.

3. Naglah, A.M.; Askar, A.A.; Hassan, A.S.; Khatab, T.K.; Al-Omar, M.A.; Bhat, M.A. biological evaluation and molecular docking with *in silico* physicochemical, pharmacokinetic and toxicity prediction of pyrazolo[1,5-*a*]pyrimidines. *Molecules* **2020**, 25, 1431.
4. Al-Wasidi, A.S.; Hassan, A.S.; Naglah, A.M. *In vitro* cytotoxicity and druglikeness of pyrazolines and pyridines bearing benzofuran moiety. *J. App. Pharm. Sci*. **2020**, 10, 142-148.
5. Kaping, S.; Boiss, I.; Singha, L.I.; Helissey, P.; Vishwakarma, J.N. A facile, regioselective synthesis of novel 3-(*N*-phenylcarboxamide)pyrazolo[1,5-*a*]pyrimidine analogs in the presence of KHSO4 in aqueous media assisted by ultrasound and their antibacterial activities. *Mol. Divers.* **2016**, 20, 379-390.
6. Hassan, A.S.; Mady, M.F.; Awad, H.M.; Hafez, T.S. Synthesis and antitumor activity of some new pyrazolo[1,5-*a*]pyrimidines. *Chin. Chem. Lett.* **2017**, 28, 388-393.
7. Parry, D.; Guzi, T.; Shanahan, F.; Davis, N.; Prabhavalkar, D.; Wiswell, D.; Seghezzi, W.; Paruch, K.; Dwyer, M.P.; Doll, R.; Nomeir, A.; Windsor, W.; Fischmann, T.; Wang, Y.; Oft, M.; Chen, T.; Kirschmeier, P.; Lees, E.M. Dinaciclib (SCH 727965), a novel and potent cyclin-dependent kinase inhibitor. *Mol. Cancer Ther.* **2010**, 9, 2344-2353.
8. Ignatova, M.; Stoyanova, N.; Manolova, N.; Rashkov, I.; Kukeva, R.; Stoyanova, R.; Toshkova, R.; Georgieva, A. Electrospun materials from polylactide and Schiff base derivative of Jeffamine ED® and 8-hydroxyquinoline-2-carboxaldehyde and its complex with Cu^{2+}: Preparation, antioxidant and antitumor activities. *Mater. Sci. Eng. C. Mater. Biol. Appl.* **2020**, 116, 111185.
9. Sahoo, J.; Sahoo, C.R.; Sarangi, P.K.N.; Prusty, S.K.; Padhy, R.N.; Paidesetty, S.K. Molecules with versatile biological activities bearing antipyrinyl nucleus as pharmacophore. *Eur. J. Med. Chem.* **2020**, 186, 111911.
10. Hassan, A.S.; Askar, A.A.; Naglah, A.M.; Almehizia, A.A.; Ragab, A. discovery of new Schiff bases tethered pyrazole moiety: design, synthesis, biological evaluation, and molecular docking study as dual targeting DHFR/DNA Gyrase inhibitors with immunomodulatory activity. *Molecules* **2020**, 25, 2593.
11. Attia, M.H.; Elrazaz, E.Z.; El-Emam, S.Z.; Taher, A.T.; Abdel-Aziz, H.A.; Abouzid, K.A.M. Synthesis and *in-vitro* anti-proliferative evaluation of some pyrazolo[1,5-*a*]pyrimidines as novel larotrectinib analogs. *Bioorg. Chem.* **2020**, 94, 103458.
12. Lv, X.-H.; Ren, Z.-L.; Li, D.-D.; Ruan, B.-F.; Li, Q.-S.; Chu, M.-J.; Ai, C.-Y.; Liu, D.-H.; Mo, K.; Cao, H.-Q. Discovery of novel double pyrazole Schiff base derivatives as anti-tobacco mosaic virus (TMV) agents. *Chin. Chem. Lett*. **2017**, 28, 377-382.
13. Bari, A.; Grenier, D.; Azelmat, J.; Syed, S.A.; Al-Obaid, A.M.; Hosten, E.C. Synthesis and anti-inflammatory activity of diversified heterocyclic systems. *Chem. Biol. Drug Des*. **2019**, 94, 1750-1759.
14. Rudrapal, M.; Celik, I.; Chinnam, S.; Ansari, M.A.; Khan, J.; Alghamdi, S.; Almehmadi, M.; Zothantluanga, J.H.; Khairnar, S.J. Phytocompounds as potential inhibitors of SARS-CoV-2 M^{pro} and PL^{pro} through computational studies. *Saudi J. Biol. Sci.* **2022**, 29, 3456-3465.
15. Ou-Yang, S.S.; Lu, J.Y.; Kong, X.Q.; Liang, Z.J.; Luo, C.; Jiang, H. Computational drug discovery. *Acta Pharmacol. Sin*. **2012**, 33, 1131-1140.
16. El-Kalyoubi, S.A.; Ragab, A.; Abu Ali, O.A.; Ammar, Y.A.; Seadawy, M.G.; Ahmed, A.; Fayed, E.A. One-pot synthesis and molecular modeling studies of new bioactive spiro-oxindoles based on uracil derivatives as SARS-CoV-2 inhibitors targeting RNA polymerase and spike glycoprotein. *Pharmaceuticals* **2022**, 15, 376.
17. Ragab, A.; Ammar, Y.A.; Ezzat, A.; Mahmoud, A.M.; Mohamed, M.B.I.; El-Tabl, A.S.; Farag, R.S. Synthesis, characterization, thermal properties, antimicrobial evaluation, ADMET study, and molecular docking simulation of new mono Cu(II) and Zn(II) complexes with 2-oxoindole derivatives, *Comput. Biol. Med*. **2022**, 145, 105473.
18. Ibrahim, S.A.; Rizk, H.F.; Aboul-Magd, D.S.; Ragab, A. Design, synthesis of new magenta dyestuffs based on thiazole azomethine disperse reactive dyes with antibacterial potential on both dyes and gamma-irradiated dyed fabric. *Dyes Pigm.* **2021**, 193, 109504.

19. Hassan, A.S.; Moustafa, G.O.; Morsy, N.M.; Abdou, A.M.; Hafez, T.S. Design, synthesis and antibacterial activity of *N*-aryl-3-(arylamino)-5-(((5-substituted furan-2-yl)methylene) amino)-1*H*-pyrazole-4-carboxamide as Nitrofurantoin® analogues. *Egypt. J. Chem.* **2020**, 63, 4469-4481.
20. Hassan, A.S.; Hafez, T.S. Antimicrobial activities of ferrocenyl complexes: A review. *J. App. Pharm. Sci.* **2018**, 8, 156-165.
21. Mukhtar, S.S.; Hassan, A.S.; Morsy, N.M.; Hafez, T.S.; Hassaneen, H.M.; Saleh, F.M. Overview on synthesis, reactions, applications, and biological activities of Schiff bases. *Egypt. J. Chem.* **2021**, 64, 6541-6554.
22. Hassan, A.S.; Osman, S.A.; Hafez, T.S. 5-Phenyl-2-furaldehyde: Synthesis, reactions and biological activities. *Egypt. J. Chem.* **2015**, 58, 113-139.
23. Morsy, N.M.; Hassan, A.S.; Hafez, T.S.; Mahran, M.R.H.; Sadawe, I.A.; Gbaj, A.M. Synthesis, antitumor activity, enzyme assay, DNA binding and molecular docking of Bis-Schiff bases of pyrazoles. *J. Iran. Chem. Soc*. **2021**, 18, 47-59.
24. Khatab, T.K.; Kandil, E.M.; Elsefy, D.E.; El-Mekabaty, A. A one-pot multicomponent catalytic synthesis of new 1*H*-pyrazole-1-carbothioamide derivatives with molecular docking studies as COX-2 inhibitors. *Biointerface Res. Appl. Chem.* **2021**, 11, 13779-1378.
25. Khatab, T.K.; Abdelghany, A.M.; Kandil, E.M.; Elsefy, D.E.; El-Mekabaty, A. Hydroxyapatite/$ZnCl_2$ nano-flakes: An efficient catalyst for the synthesis of 2-arylbenzothiazoles with molecular docking and anti-oxidant evaluation. *Biointerface Res. Appl. Chem.* **2020**, 10, 5182-5187.
26. Khatab, T.K.; Mubarak, A.Y.; Soliman, H.A. Design and synthesis pairing between xanthene and tetrazole in pentacyclic system using tetrachlorosilane with aurora kinase inhibitor validation. *J. Heterocycl. Chem*. **2017**, 54, 2463-2470.
27. Khatab, T.K.; Hassan, A.S.; Hafez, T.S. V_2O_5/SiO_2 as an efficient catalyst in the synthesis of 5-aminopyrazole derivatives under solvent free condition. *Bull. Chem. Soc. Ethiop.* **2019**, 33, 135-142.
28. Hassan, A.S.; Moustafa, G.O.; Awad, H.M.; Nossier, E.S.; Mady, M.F. Design, synthesis, anticancer evaluation, enzymatic assays, and a molecular modeling study of novel pyrazole–indole hybrids. *ACS Omega* **2021**, 6, 12361-12374.
29. Hassan, A.S.; Awad, H.M.; Magd-El-Din, A.A.; Hafez, T.S. Synthesis and in vitro antitumor evaluation of novel Schiff bases. *Med. Chem. Res*. **2018**, 27, 915-927.
30. El-Naggar, M.; Hassan, A.S.; Awad, H.M.; Mady, M.F. Design, synthesis and antitumor evaluation of novel pyrazolopyrimidines and pyrazoloquinazolines. *Molecules* **2018**, 23, 1249.
31. Hassan, A.S. Antimicrobial evaluation, in silico ADMET prediction, molecular docking, and molecular electrostatic potential of pyrazole-isatin and pyrazole-indole hybrid molecules. *J. Iran. Chem. Soc*. **2022**, 19, 3577-3589.
32. Gasmi, A., Peana, M., Noor, S.; Lysiuk, R.; Menzel, A.; Benahmed, A.G.; Bjørklund, G. Chloroquine and hydroxychloroquine in the treatment of COVID-19: The never-ending story. *Appl. Microbiol. Biotechnol.* **2021**, 105, 1333-1343.
33. Abdel-Latif, E.; Khatab, T.K.; Fekri, A.; Khalifa, M.E. Synthesis of new binary thiazole-based heterocycles and their molecular docking study as COVID-19 main protease (M^{pro}) inhibitors. *Russ. J. Gen. Chem.* **2021**, 91, 1767-1773.
34. Hwang, J.; Youn, K.; Ji, Y.; Lee, S.; Lim, G.; Lee, J.; Ho, C.-T.; Leem, S.-H.; Jun, M. Biological and computational studies for dual cholinesterases inhibitory effect of zerumbone. *Nutrients* **2020**, 12, 1215.
35. Daina, A.; Michielin, O.; Zoete, V. SwissADME: a free web tool to evaluate pharmacokinetics, drug-likeness and medicinal chemistry friendliness of small molecules. *Sci Rep.* **2017**, 7, 42717.